Fuel 230 (2018) 440–451

Contents lists available at ScienceDirect

Fuel

journal homepage: www.elsevier.com/locate/fuel

Full Length Article

High efficiency ethanol-diesel dual-fuel combustion: A comparison against conventional diesel combustion from low to full engine load

Vinícius B. Pedrozo*, Ian May, Wei Guan, Hua Zhao

Centre for Advanced Powertrain and Fuels Research (CAPF), Brunel University London, Kingston Lane, Uxbridge, Middlesex UB8 3PH, United Kingdom

ARTICLE INFO

Keywords:
Ethanol
Low carbon fuel
Dual-fuel combustion
Diesel engine
Greenhouse gas emissions

ABSTRACT

Comparisons between dual-fuel combustion and conventional diesel combustion (CDC) are often performed using different engine hardware setups, exhaust gas recirculation rates, as well as intake and exhaust manifold pressures. These modifications are usually made in order to curb in-cylinder pressure rise rates and meet exhaust emissions targets during the dual-fuel operation. To ensure a fair comparison, an experimental investigation into dual-fuel combustion has been carried out from low to full engine load with the same engine hardware and identical operating conditions to those of the CDC baseline. The experiments were executed on a single cylinder heavy-duty diesel engine at a constant speed of 1200 rpm and various steady-state loads between 0.3 and 2.4 MPa net indicated mean effective pressure (IMEP). Ethanol was port fuel injected while diesel was direct injected using a high pressure common rail injection system. The start of diesel injection was optimised for the maximum net indicated efficiency in both combustion modes. Varied ethanol energy fractions and different diesel injection strategies were required to control the in-cylinder pressure rise rate and achieve highly efficient and clean dual-fuel operation. In terms of performance, dual-fuel combustion attained higher net indicated efficiency than the CDC mode from 0.6 to 2.4 MPa IMEP, with a maximum value of 47.2% at 1.2 MPa IMEP. The comparison also shows the use of ethanol resulted in 26% to 90% lower nitrogen oxides (NOx) emissions than the CDC operation. At the lowest engine load of 0.3 MPa IMEP, the dual-fuel operation led to simultaneous low NOx and soot emissions at the expense of a relatively low net indicated efficiency of 38.9%. In particular, the reduction in NOx emissions introduced by the utilisation of ethanol has the potential to decrease the engine running costs via lower consumption of aqueous urea solution in the selective catalyst reduction system. Moreover, the dual-fuel combustion with a low carbon fuel such as ethanol is an effective means of decreasing the use of fossil fuel and associated greenhouse gas emissions.

1. Introduction

Heavy-duty (HD) vehicles are typically powered by diesel engines due to their cost-effectiveness and high fuel conversion efficiency. However, there is a lot of concern over the greenhouse gas (GHG) emissions produced from the combustion of diesel and other fossil fuels [1]. This is due to a recent increase in the atmospheric concentration of GHGs such as carbon dioxide (CO_2) [2], which can cause irreversible

Abbreviations: ATDC, after firing top dead centre; CA10, crank angle of 10% cumulative heat release; CA10–CA90, combustion duration or 10–90% cumulative heat release; CA50, crank angle of 50% cumulative heat release; CA90, crank angle of 90% cumulative heat release; CAD, crank angle degree; CDC, conventional diesel combustion; CH4, methane; CO, carbon monoxide; CO2, carbon dioxide; CO2eq, CO_2 equivalent; COV_IMEP, coefficient of variation of IMEP; COV_Pmax, coefficient of variation of P_{max}; DAQ, data acquisition; ECR, effective compression ratio; ECU, engine control unit; EF, ethanol energy fraction; EGR, exhaust gas recirculation; EGT, exhaust gas temperature; FID, flame ionisation detector; FSN, filter smoke number; GHG, greenhouse gas; GWP, global warming potential; HC, hydrocarbons; HD, heavy-duty; HRR, apparent net heat release rate; iEGR, internal EGR; iLUC, indirect land use change; IMEP, net indicated mean effective pressure; ISCO, net indicated specific emissions of CO; $ISCO_2$, net indicated specific emissions of CO_2; ISHC, net indicated specific emissions of actual unburnt HC; ISNOx, net indicated specific emissions of NOx; LHV_{diesel}, lower heating value of diesel; $LHV_{ethanol}$, lower heating value of ethanol; LHV_{fuel}, lower heating value; $\dot{m}_{air}$, fresh air mass flow rate; $\dot{m}_{diesel}$, diesel mass flow rate; $\dot{m}_{ethanol}$, ethanol mass flow rate; $\dot{m}_{urea}$, estimated consumption of aqueous urea solution in the SCR system; M_{CO_2}, normalised molar mass of CO_2; M_{diesel}, normalised molar mass of diesel; $M_{ethanol}$, normalised molar mass of ethanol; M_{fuel}, normalised molar mass; MFB, mass fraction burnt; N_2O, nitrous oxide; *Net Indicated Eff.*$_{SCRcorr.}$, SCR corrected net indicated efficiency; NOx, nitrogen oxides; O_2, Oxygen; P_{ind}, net indicated power; PFI, port fuel injector; P_{max}, peak in-cylinder gas pressure; PRR, pressure rise rate; RON, research octane number; SCR, selective catalyst reduction; SOC, start of combustion; SOI_main, actual start of main diesel injection; SOI_mai–SOC, ignition delay; SOI_pre, actual start of diesel pre-injection; TDC, firing top dead centre; TTW, tank-to-wheels; VVA, variable valve actuation; WTT, well-to-tank; WTT_{diesel}, WTT CO_{2eq} emissions for fossil diesel; $WTT_{ethanol}$, WTT CO_{2eq} emissions for ethanol; WTW, well-to-wheels; $\%C_{fuel}$, carbon mass content; $\%H_{fuel}$, hydrogen mass content; $\%O_{fuel}$, carbon mass content; γ, ratio of specific heats; ρ_{fuel}, density; ρ_{diesel}, diesel density; $\rho_{ethanol}$, ethanol density; Φ, global fuel/air equivalence ratio

* Corresponding author.
E-mail address: vinicius.pedrozo@brunel.ac.uk (V.B. Pedrozo).

https://doi.org/10.1016/j.fuel.2018.05.034
Received 19 February 2018; Received in revised form 5 May 2018; Accepted 8 May 2018
Available online 25 May 2018

climate change and negatively impact the health of living organisms across the globe [1].

In 2010, HD vehicles were responsible for approximately 34% of the GHGs emitted by the global transport sector and 46.5% of the road transport CO_2 emissions [3]. This disproportionate contribution is highlighted by the fact the HD fleet represents only 11% of the world motor vehicles [4]. Substantial and continuous reduction in fossil fuel energy use and GHG emissions must be achieved in order to address the transport sector's impact on the environment.

Additional cause for concern is that CDC is prone to a wide range of local in-cylinder gas temperatures and fuel/air equivalence ratios that can lead to the formation of noxious emissions, such as NOx and soot [5,6]. NOx emissions are mainly formed in near-stoichiometric high temperatures regions close to the diesel diffusion flame [7]. Soot formation occurs in high fuel/air equivalence ratio and intermediate temperature zones within the diesel spray [8,9]. These pollutants are linked to premature deaths caused by cardiovascular and respiratory diseases [10,11].

Stringent fuel conversion efficiency and exhaust emissions regulations have been implemented to limit the levels of GHG and noxious emissions from HD vehicles [12–15]. Manufacturers are incorporating costly engine design elements [16–20] and aftertreatment technologies [21,22] to comply with the aforementioned emissions standards and GHG targets [12,13]. The use of improved selective catalyst reduction (SCR) systems for NOx mitigation, flexible and high pressure diesel injection equipment, as well as high efficiency turbocharging and air handling systems are some of the ways in which this is being achieved.

Reaching a balance between engine running costs and exhaust emissions can represent a challenge for HD engine manufacturers [16,17]. Both in-cylinder and aftertreatment measures are considered and are often linked. An improvement of 1% in fuel conversion efficiency can increase the levels of engine-out NOx from 10 g/kWh to 14 g/kWh [18]. This adversely affects the total cost of ownership due to a higher consumption of aqueous urea solution in the SCR system [23–26]. On the other hand, CDC operation with very low engine-out NOx emissions can result in low fuel conversion efficiency and excessive levels of soot due the different formation mechanisms [27,28].

Previous studies into dual-fuel compression ignition combustion have demonstrated that the strategy has the potential to resolve these issues, increasing the fuel conversion efficiency while decreasing both the NOx and soot emissions [6,29–32]. This has been attributed to simultaneous reductions in local fuel/air equivalence ratio and temperature, shorter combustion duration, and lower heat transfer losses [6,32].

Fig. 1 shows an example of a dual-fuel system, which can be achieved by the installation of a port fuel injection system of a low reactivity fuel such as gasoline [32], ethanol [33], or natural gas [34] on a diesel engine. The ignition of the premixed charge is generally triggered by direct injections of diesel [6,35]. It should be noted that the use of a low carbon fuel like ethanol [36–39] can help decrease the dependence on fossil fuels and minimise GHG emissions from the global transport sector [40].

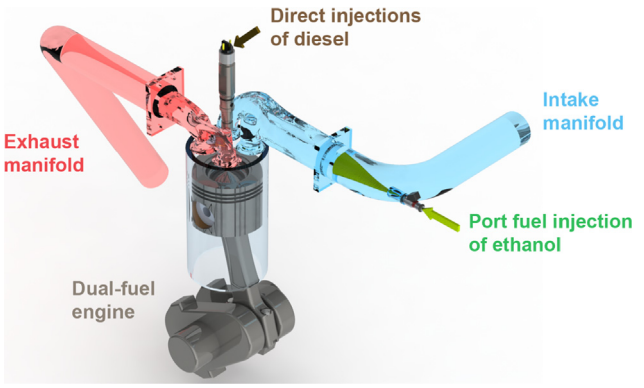

Fig. 1. Schematic diagram of a dual-fuel engine with direct injections of diesel and port fuel injection of ethanol.

Despite the advantages of dual-fuel operation, it is challenging to obtain direct comparisons against the CDC mode from low to high engine loads (e.g. above 2.0 MPa IMEP). This is often due to modifications in engine hardware and/or test conditions that are used to control the emissions of NOx and the in-cylinder pressure rise rates from dual-fuel combustion. These alterations typically include the use of a different piston design and/or compression ratio [41,42] as well as changes in the levels of exhaust gas recirculation [43].

This study aims to explore the potential of ethanol–diesel dual-fuel combustion to achieve high fuel conversion efficiency and low exhaust emissions using the same combustion system and identical engine testing conditions to those of the CDC baseline. To the best of our knowledge, this is the first attempt to experimentally compare the controllability, emissions, and fuel conversion efficiency of the above-mentioned combustion modes from low to full engine load (e.g. 0.3–2.4 MPa IMEP). In addition to this, practical considerations have been raised and the potential CO_2 reduction has been discussed on both a tank-to-wheels and well-to-wheels basis [37,44].

The investigation was performed on a single cylinder HD diesel engine at a steady-state speed of 1200 rpm. The diesel injection timings and the number of injections per cycle were optimised in both the combustion modes in order to maximise the fuel conversion efficiency, which was given by the net indicated efficiency. Moreover, dual-fuel operation was carried out using ethanol energy fractions that achieved the highest net indicated efficiency with minimal NOx and soot emissions, as determined in our previous studies [29–31,45,46].

2. Experimental setup

2.1. Experimental facilities

A schematic diagram of the single cylinder HD engine experimental setup is shown in Fig. 2. A Froude Hofmann AG150 eddy current dynamometer was used to absorb the power produced by the engine. Fresh intake air was supplied to the engine via an AVL 515 sliding vanes compressor with a closed loop control for the boost pressure. A throttle valve located upstream of a surge tank provided fine control over the intake manifold pressure. The fresh air mass flow rate ($\dot{m}_{air}$) was measured with an Endress + Hauser Proline t-mass 65F thermal mass flow meter.

Another surge tank was installed in the exhaust manifold to damp out pressure fluctuations prior to the exhaust gas recirculation (EGR) circuit. An electronically controlled butterfly valve located downstream of the exhaust surge tank was used to set the required back pressure (e.g. exhaust manifold pressure). High-pressure loop cooled external EGR was supplied to the engine intake system by opening a pulse width modulation-controlled EGR valve. Boosted intake air and external EGR temperatures were controlled using water cooled heat exchangers.

2.2. Engine specifications

Base hardware specifications are outlined in Table 1. The combustion system consisted of a 4-valve swirl-oriented cylinder head and a stepped-lip piston bowl design with a geometric compression ratio of 16.8.

The diesel introduction was controlled via a dedicated engine control unit (ECU) with the ability to support up to three injections per cycle. The intake valve lift profile was adjusted via a lost-motion variable valve actuation (VVA) system based on a normally open high-speed solenoid valve assembly and a special intake cam design [47].

Coolant and oil pumps were not coupled to the engine and were driven by separate electric motors. Engine coolant and oil temperatures

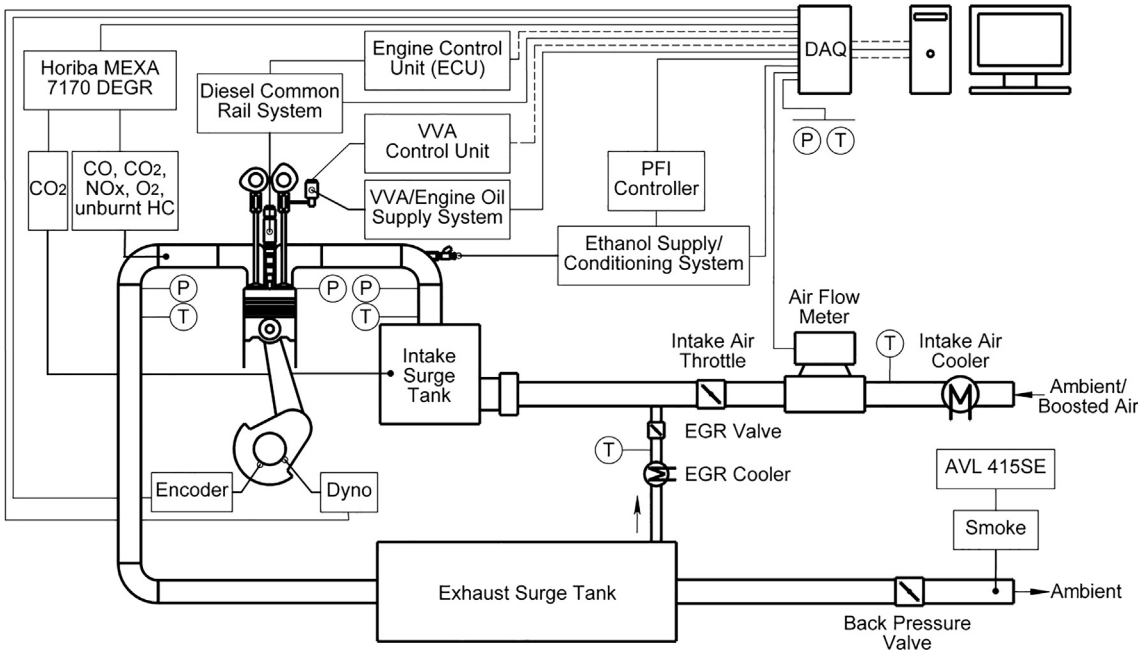

Fig. 2. Schematic diagram of the engine experimental setup.

Table 1
Single cylinder HD engine specifications.

Parameter	Value
Displaced volume	2.026 dm^3
Stroke	155 mm
Bore	129 mm
Connecting rod length	256 mm
Number of valves	4
Piston type	Stepped-lip bowl
Geometric compression ratio	16.8
Peak in-cylinder pressure (P_{max}) limitation	18 MPa
Diesel injection system	Bosch common rail, injection pressure of 50–220 MPa, 8 holes with nominal diameter of 0.176 mm, included spray angle of 150°
Ethanol injection system	PFI Marelli IWP069, included spray angle of 15°

were set to 353 ± 3 K. The oil pressure was held at 450 ± 10 kPa throughout the experiments.

2.3. Fuel properties and delivery

The relevant properties of the fuel used in this work are listed in Table 2. The diesel fuel was supplied to the engine using a high pressure common rail injection system. Two Endress + Hauser Promass 83A Coriolis flow meters were used to determine the diesel mass flow rate ($\dot{m}_{diesel}$) by measuring the total fuel supplied to and from the diesel high pressure pump and injector.

While the use of two fuel flow meters is not ideal due to the compounding of measurement error, this setup was the only option for regulating the backpressure on the diesel injector return line. Tests were carried out to validate the consistency of the diesel fuel measurements with two fuel flow meters, achieving a combined uncertainty [48,49] smaller than ± 1.7%.

In order to enable dual-fuel operation, an ethanol fuel injection system was designed and fitted to the engine. Ethanol was injected through a port fuel injector (PFI) installed in the intake manifold. An in-house injector driver controlled the injector pulse width, which was adjusted according to the desired ethanol energy fraction.

The ethanol mass flow rate ($\dot{m}_{ethanol}$) was measured using an Endress + Hauser Proline Promass 80A Coriolis flow meter, allowing for measurements with an accuracy of ± 0.15% of reading. The injection pressure was continuously monitored by a pressure transducer, so that a constant relative pressure of 300 kPa could be maintained across the injector.

Table 2
Fuel properties.

Property	Diesel	Ethanol
Product name	Red diesel (gas oil)	Absolute ethanol 100
Standard/specification	BS 2869 Class A2	Anhydrous ethanol
Density at 293 K (ρ_{fuel})	0.827 kg/dm^3	0.790 kg/dm^3 [50]
Cetane number	> 45	n/a
Research octane number (RON)	n/a [51]	~107 [51]
Alcohol content in volume	n/a	99.9%
Water content	< 0.20 g/kg [52]	1.7 g/kg [50]
Sulphur content	< 0.01 g/kg	n/a
Heat of vaporisation	270 kJ/kg [51]	840 kJ/kg [51]
Carbon mass content (%C_{fuel})	86.6%	52.1% [51]
Hydrogen mass content (%H_{fuel})	13.2%	13.1% [51]
Oxygen mass content (%O_{fuel})	0.2%	34.8% [51]
Normalised molecular composition	$CH_{1.825}O_{0.0014}$	$CH_3O_{0.5}$
Lower heating value (LHV_{fuel})	42.9 MJ/kg	26.9 MJ/kg [51]

2.4. Exhaust emissions measurements and analysis

Gaseous emissions such as NOx, CO_2, carbon monoxide (CO), oxygen (O_2), and unburnt hydrocarbon (HC) were taken with a Horiba MEXA-7170 DEGR emissions analyser. The EGR rate was determined by calculating the ratio of the intake to the exhaust manifold CO_2 concentration measured by the same emissions analyser. A high pressure module allowed for high-pressure sampling upstream of the back pressure valve while a heated line was used to prevent water condensation.

The measurement of unburnt HC was performed on a wet basis by the Horiba's heated flame ionisation detector (FID). However, the HC emissions measured with the FID can lead to misinterpretation of the results due to the relative insensitivity of the device towards alcohols and aldehydes [53,54]. Therefore, the FID response was corrected by the method developed by Kar and Cheng [53] with an updated response factor of 0.68 for the oxygenated organic species resultant from ethanol combustion [54]. This procedure has been reported in our previous work [31] and allows for the determination of the actual unburnt HC emissions.

The concentration of NOx, CO, and unburnt HC in the exhaust stream were converted from parts per million (ppm) to net indicated specific emissions using the methodology described in the Regulation number 49 of the Economic Commission for Europe of the United Nations [52]. NOx and CO were converted to a wet basis by applying a correction factor for the raw exhaust gas according to the in-cylinder fuel mixture composition.

An AVL 415SE smoke meter was used to measure the concentration of black carbon containing soot. The measurements were reported on a filter smoke number (FSN) basis, as previous studies [55–58] have reported that low levels of soot from dual-fuel combustion do not correlate well with the amount of particle mass produced. The actual particle mass is expected to be higher, particularly at low engine loads, because semi-volatile organic species can condense on small solid cores (e.g. carbonaceous) [59].

2.5. Data acquisition

The in-cylinder pressure was measured by a Kistler 6125C piezoelectric pressure sensor coupled with an AVL FI Piezo charge amplifier. Intake and exhaust manifold pressures were measured by two Kistler 4049A water cooled piezoresistive absolute pressure sensors coupled to Kistler 4622A amplifiers. Temperatures and pressures at relevant locations were measured by K-type thermocouples and pressure gauges, respectively.

Two National Instruments data acquisition (DAQ) cards and a personal computer were used to acquire the signals from the measurement device. A USB-6251 high speed DAQ card received the crank angle resolved data synchronized with an optical encoder of 0.25 crank angle degrees (CAD) resolution. A USB-6210 low speed DAQ card acquired the low frequency engine operation conditions. These data were displayed live by an in-house developed DAQ program and combustion analyser.

2.6. Data analysis

A relevant parameter for the dual-fuel operation was the ethanol energy fraction (EF), which was defined as the ratio of the energy content of the ethanol to the total fuel energy supplied by

$$EF = \frac{\dot{m}_{ethanol} LHV_{ethanol}}{(\dot{m}_{ethanol} LHV_{ethanol}) + (\dot{m}_{diesel} LHV_{diesel})} \quad (1)$$

The global fuel/air equivalence ratio (Φ) was given by

$$\phi = \frac{(14.5\dot{m}_{diesel} + 9.0\dot{m}_{ethanol})}{\dot{m}_{air}} \quad (2)$$

Crank angle based in-cylinder pressure traces were averaged over 200 consecutive cycles for each operating point and used to calculate the IMEP and the apparent net heat release rate (HRR). The pressure rise rate (PRR) was represented by the average of the maximum pressure variations of 200 cycles of cylinder pressure versus crank angle. Combustion and in-cylinder flow stability were monitored by the coefficient of variation of IMEP (COV_IMEP) and P_{max} (COV_P_{max}) over the sampled cycles.

Since the absolute value of the heat released is not as important to this study as the bulk shape of the curve with respect to crank angle, a constant ratio of specific heats (γ) of 1.33 was assumed throughout the engine cycle. The mass fraction burnt (MFB) was given by the ratio of the integral of the HRR and the maximum cumulative heat release. Combustion phasing was determined by the crank angle of 50% (CA50) cumulative heat release. Combustion duration was represented by the period of time between the crank angles of 10% (CA10) and 90% (CA90) cumulative heat release.

A current probe was used to acquire the electric current signal sent from the ECU to the diesel injector solenoid. The signal was corrected by adding the respective energising time delay, which was previously measured in a constant volume chamber [60]. The resulting diesel injector current signal allowed for the determination of the actual start of diesel injection.

Ignition delay was defined as the period of time between the actual start of main diesel injection (SOI_main) and the start of combustion (SOC), set to 0.3% MFB point of the averaged cycle. After the calculation of the combustion characteristics (e.g. CA50) and ignition delay, the average in-cylinder pressure and the resulting HRR were smoothed using a Savitzky-Golay filter.

Net indicated efficiency was determined by calculating the ratio of the net indicated power to the rate of fuel energy supplied to the engine. Combustion efficiency calculations were based on the emissions products not fully oxidised during the combustion process except soot using the method reported in [46].

3. Methodology

Fig. 3 shows the location of the test points over an estimated speed and load map of a HD diesel engine. Testing was carried out under a steady-state engine speed of 1200 rpm over a range of loads from 0.3 to 2.4 MPa IMEP. A PRR of 2.0 MPa/CAD and a P_{max} of 18 MPa were considered as the upper bounds for calibration. Stable engine operation was quantified by COV_IMEP values < 5%.

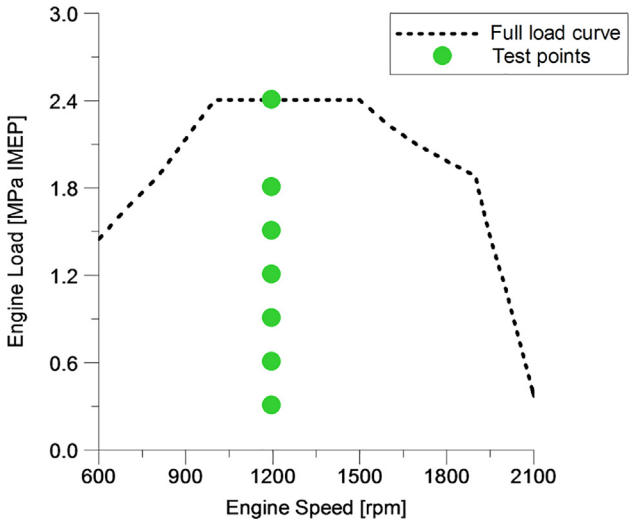

Fig. 3. Experimental test points over an estimated HD diesel engine speed-load map.

Table 3
Operating conditions for the CDC and ethanol–diesel dual-fuel operation from low to full engine load at 1200 rpm.

Engine load	Intake manifold pressure	Exhaust manifold pressure	Intake manifold air temp.	EGR rate	Diesel injection pressure (CDC)	Diesel injection pressure (Dual-fuel)
MPa IMEP	kPa	kPa	K	%	MPa	MPa
0.3	115	125	307	25	105	50
0.6	125	135	310	25	125	90
0.9	155	165	315	25	140	110
1.2	190	200	319	25	155	125
1.5	230	240	324	25	170	140
1.8	260	270	324	20	190	160
2.4	300	310	323	11	220	190

The experiments were performed with a pressure-based effective compression ratio (ECR) of 16.8 [46]. The ECR was calculated using the effective in-cylinder volume at intake valve closing, which was obtained from the intersection of the intake manifold pressure and an extrapolated polytropic compression curve fitted to the experimental in-cylinder pressure [61,62]. The expansion ratio remained constant as a result of the fixed exhaust camshaft timing.

Table 3 summarises the test conditions for the CDC and ethanol–diesel dual-fuel operating modes. The intake manifold pressure set point was taken from a Euro V compliant multi-cylinder HD diesel engine in order to provide a sensible starting point, since an external boosting device was used in place of a turbocharger. The exhaust manifold pressure was varied to maintain a constant pressure differential across the cylinder of 10 kPa. This difference of 10 kPa between exhaust and intake manifold pressures was used to simulate the pumping losses typically associated with a turbocharger and to drive the requested amounts of EGR.

The EGR rate was held constant at a given engine load in order to ensure a fair comparison between CDC and dual-fuel operation. The EGR rate was limited at 25% between 0.3 and 1.5 MPa IMEP to avoid excessive smoke and a decrease in net indicated efficiency. At 1.8 and 2.4 MPa IMEP, the EGR rate was reduced to 20% and 11%, respectively. This was required to achieve lean and efficient high load operation using the same levels of boost pressure as the multi-cylinder engine.

Diesel injection pressures were set to be 30 to 55 MPa higher in the CDC mode than those in the dual-fuel combustion due to the relatively higher diesel flow rates and longer injection durations at a given engine load. This was necessary to minimise soot emissions from the CDC operation via improved diesel atomisation and enhanced the fuel–air mixing process. The use of the same diesel injection pressure on the dual-fuel mode could have caused overmixing at low engine loads and excessive PRR at medium and high engine loads.

All comparisons were carried out for the cases that attained the highest net indicated efficiencies after sweeps of diesel injection timings. Additionally, the diesel injection strategy (i.e. number of diesel injections per cycle) was optimised and varied as the engine load was increased. In the dual-fuel mode, the ethanol energy fraction was also optimised for minimum NOx and soot emissions, as supported by our previous dual-fuel studies [29–31,45,46]. A maximum EF of 0.79 was achieved at 1.2 MPa IMEP. Advanced dual-fuel combustion control strategies such as internal exhaust gas recirculation (iEGR) [31] and Miller cycle [46] were not explored in this study as they would require different operating conditions.

4. Results and discussion

4.1. Overview of the load sweep

Fig. 4 depicts the effect of engine load on both the operating modes. CDC operation was characterised by longer mixing-controlled combustion phase as the load was increased. This was attributed to longer diesel injection periods and increased amount of fuel, which limited the fuel vapour-air mixing process [51,63]. The optimum CA50 in CDC mode varied as the engine load was increased, allowing for more advanced burn rates at mid-loads and delayed combustion events at high loads. The reasons behind this are described in the next subsection.

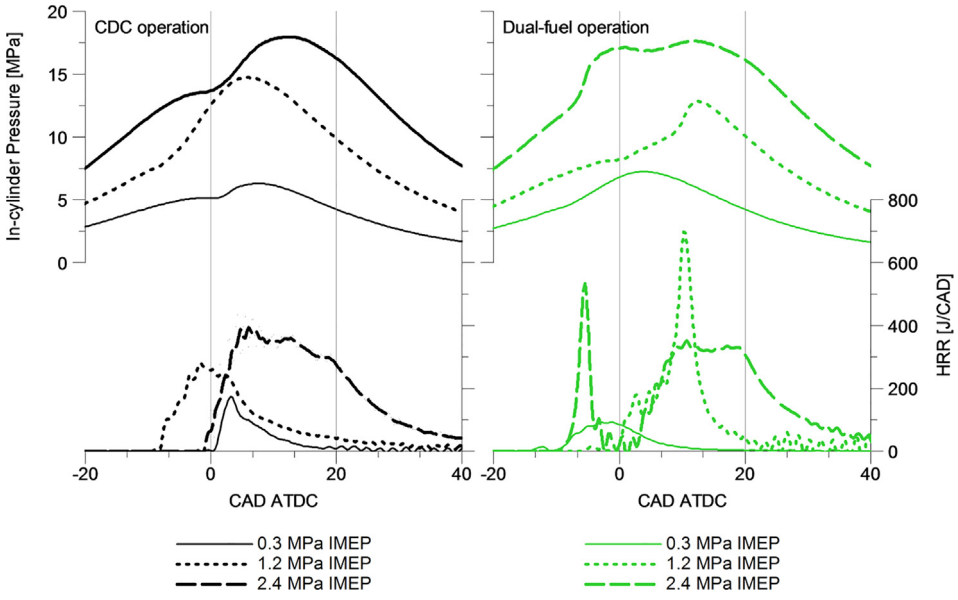

Fig. 4. The effect of engine load on CDC and ethanol–diesel dual-fuel operation at 1200 rpm.

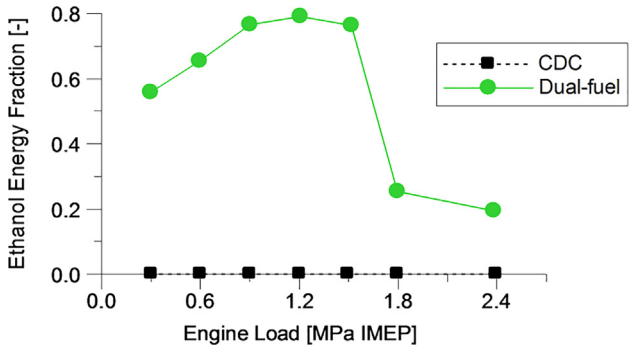

Fig. 5. Optimum ethanol energy fraction for varied engine loads at 1200 rpm.

The dual-fuel operation led to higher peak heat release than the CDC mode at all engine loads except 0.3 MPa IMEP. This required different diesel injection strategies and eventually later combustion process in order to control the PRR as the engine load was increased. The combustion was triggered by and initiated after the start of diesel injection at low and medium load operations between 0.3 and 1.5 MPa IMEP. Higher compression pressures and temperatures accelerated the autoignition of the premixed ethanol fuel prior to the diesel injection at high engine loads of 1.8 and 2.4 MPa IMEP.

Fig. 5 shows the optimum EF was rapidly reduced from 0.76 to 0.25 when increasing the engine load from 1.5 to 1.8 MPa IMEP. This was necessary in order to minimise the PRR associated with the early autoignition of ethanol. It is important to highlight that modifications in the engine hardware (e.g. lower ECR via Miller cycle) and/or test procedure (e.g. lower intake manifold air temperature) can increase the maximum EF at higher loads [46].

4.2. Combustion control

Fig. 6 shows the actual start of diesel pre-injection (SOI_pre), SOI_main, and in-cylinder pressure characteristics for optimised CDC and dual-fuel operation. In the CDC mode, a 3 mm^3 diesel pre-injection with a constant dwell time of 1 ms was used to reduce the levels of PRR [45] between the engine loads of 0.3 MPa IMEP and 1.5 MPa IMEP. The lower PRR were associated with the shorter ignition delay produced by the combustion of the diesel pre-injection, which likely formed of a hot and reactive mixture prior to the main diesel injection [64].

At high engine loads of 1.8 and 2.4 MPa IMEP, relatively shorter ignition delays introduced by lower EGR rates and higher in-cylinder pressures and temperatures allowed for the use of a single diesel injection near firing top dead centre (TDC). The maximum SOI_main advance was limited by the P_{max} while the PRR was maintained within the limit of 2.0 MPa/CAD.

In the dual-fuel operation, the combination of an early single diesel injection at about -36 CAD after top dead centre (ATDC) and ethanol energy fractions of 0.56 and 0.65 allowed for long ignition delays (SOI_main–SOC) and better mixture preparation at 0.3 and 0.6 MPa IMEP. This enhanced the combustion process via a more progressive and probably sequential combustion from high to low reactivity regions [8]. This has also been identified in computational simulations performed by Desantes et al. [65] and is supported by the low levels of PRR. However, the P_{max} was increased when compared to that of the CDC operation due to earlier CA50 and shorter combustion for the dual-fuel mode at these particular loads (see Fig. 7).

At mid-loads between 0.9 and 1.5 MPa IMEP, less partially premixed diesel fuel could be used in order to prevent an early ignition of the in-cylinder charge. Therefore, the mass of the diesel was divided into two direct injections using the same strategy employed in the CDC cases. The injection of a small amount of diesel prior to the SOI_main was essential to mitigate excessive PRR. This was a result of a shorter SOI_main–SOC period and elimination of the premixed combustion

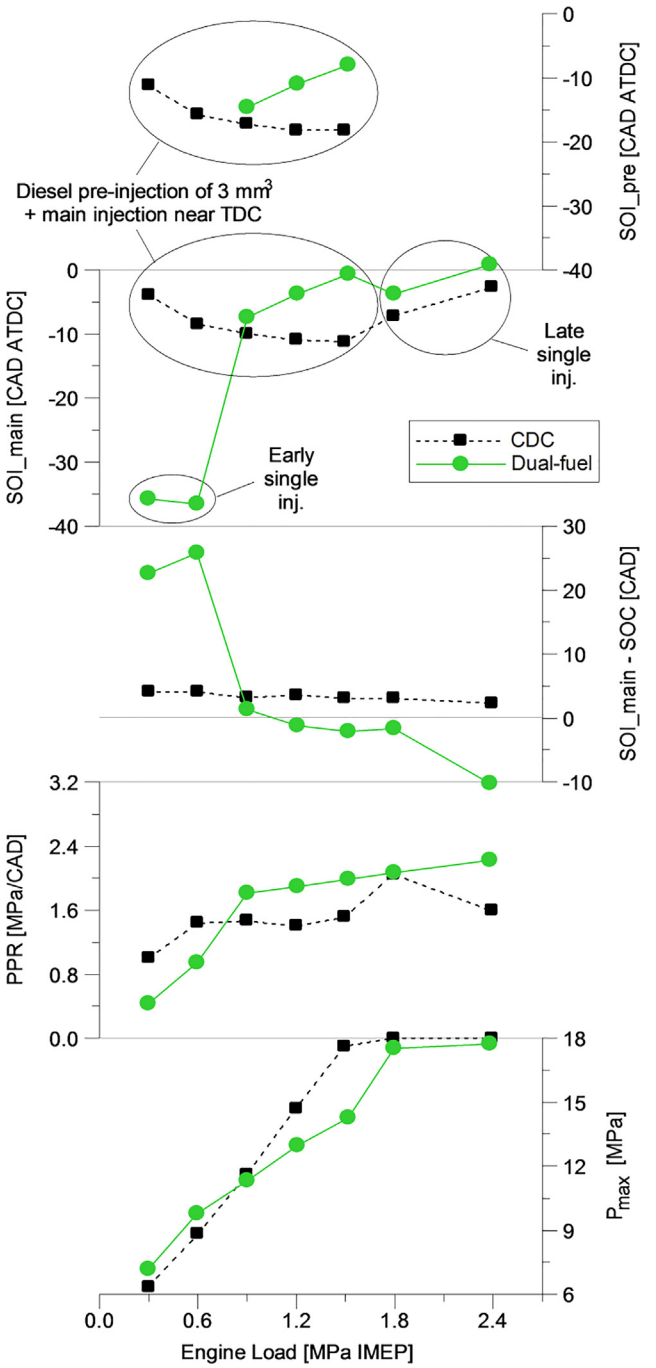

Fig. 6. Diesel injection timings and combustion characteristics for optimised CDC and ethanol–diesel dual-fuel operation at 1200 rpm.

peak typically observed with a late single diesel injection strategy [45]. Despite the controlled levels of PRR, the diesel injection timings were delayed by up to 10.5 CAD when compared to those of the CDC operation, helping to decrease the P_{max} levels.

At 1.8 and 2.4 MPa IMEP, the premixed ethanol fuel autoignited prior to the diesel injection. Low ethanol energy fractions and a single diesel injection near TDC were used to control the burn rate as well as the resulting PRR and P_{max}. The introduction of a diesel pre-injection would increase the PRR levels at these loads due to simultaneous and early combustion of the ethanol and pre-injected diesel fuel.

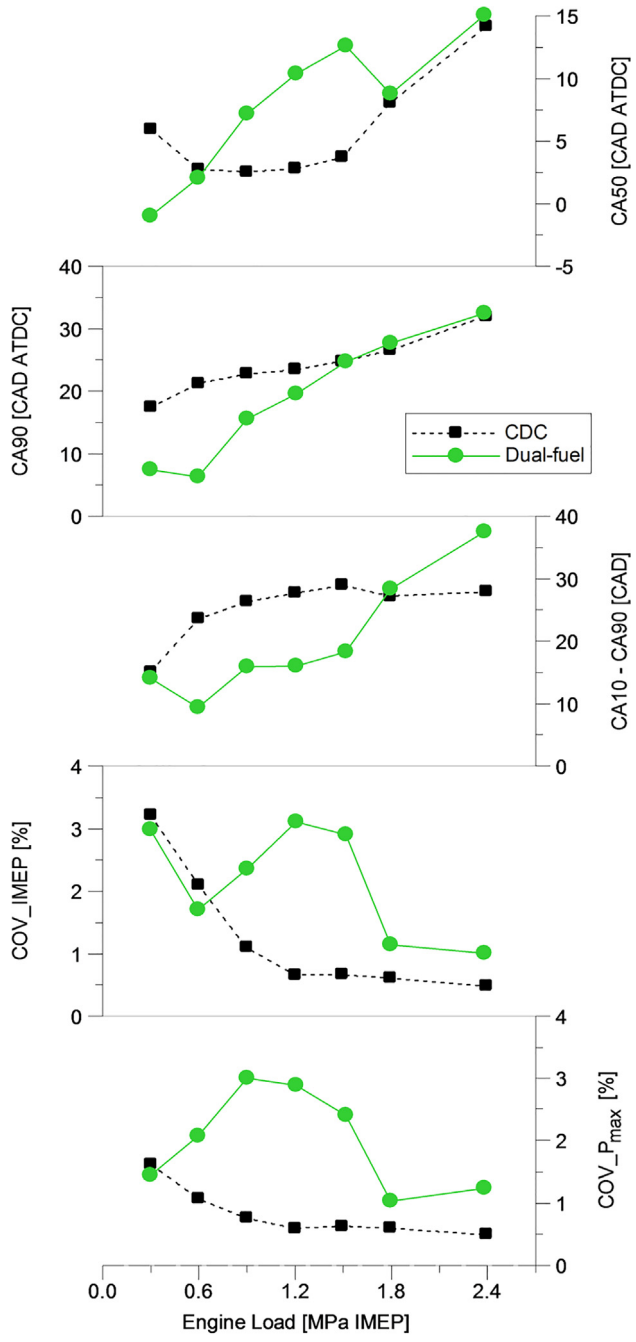

Fig. 7. Heat release characteristics for optimised CDC and ethanol–diesel dual-fuel operation at 1200 rpm.

4.3. Heat release analysis

Fig. 7 depicts the heat release characteristics for the CDC and dual-fuel operation. The optimum CA50 for the maximum net indicated efficiency was initially advanced and then retarded in the CDC mode. The advance in the CA50 when increasing the engine load from 0.3 to 0.6 MPa IMEP was likely linked to the longer CA10–CA90 period and relatively lower heat transfer losses obtained at 0.6 MPa IMEP. The CA50 delay at high load operations of 1.8 and 2.4 MPa IMEP was associated with the peak in-cylinder pressure limitation. Additionally, lower levels of EGR and higher combustion temperatures shortened the CA10–CA90 period and probably increased heat transfer losses of the CDC operation at these high load conditions.

In comparison, the dual-fuel operation often required later CA50 as the engine load was increased in order to control the PRR within the limit of 2.0 MPa/CAD. At high loads of 1.8 and 2.4 MPa IMEP, the CA50 and CA90 were similar for both the combustion modes due to the P_{max} limitation of 18 MPa and lower ethanol energy fractions used in the dual-fuel mode.

In general, an increase in engine load led to later CA90 and longer CA10–CA90 period as a result of the higher fuel flow rates. The higher degree of premixed combustion in the dual-fuel mode was likely the cause for the relatively earlier CA90 and faster CA10–CA90 period between 0.3 and 1.5 MPa IMEP. Nonetheless, the early ignition of the ethanol fuel produced longer burn rates than the CDC operation at 1.8 and 2.4 MPa IMEP.

In terms of combustion stability, the mixing-controlled combustion of the CDC operation effectively decreased the COV_IMEP and COV_P_{max} to 0.5% as the engine load was increased to 2.4 MPa IMEP. In the dual-fuel mode, later CA50 and a more premixed combustion yielded higher levels of COV_IMEP than the CDC case between 0.9 and 2.4 MPa IMEP. The increase in COV_IMEP was proportional to the EF. In addition, the dual-fuel operation resulted in higher COV_P_{max} than the CDC mode at all engine loads except 0.3 MPa IMEP. Nevertheless, the COV_IMEP and COV_P_{max} could be controlled between 1.0% and 3.0%.

4.4. Engine-out emissions

Fig. 8 shows the engine-out emissions for the optimum cases over a sweep of load. An EGR rate of 25% was used in order to minimise NOx emissions at engine loads up to 1.5 MPa IMEP. This allowed for CDC operation with net indicated specific emissions of NOx (ISNOx) of 3.9 g/kWh, on average, between 0.3 and 1.5 MPa IMEP. The use of lower EGR rates of 20% and 11% increased the combustion temperatures at 1.8 and 2.4 MPa IMEP, yielding higher ISNOx of 4.4 and 5.7 g/kWh, respectively.

Alternatively, the optimised dual-fuel operation achieved lower ISNOx than the CDC mode at all engine loads. This was linked to the premixed ethanol fuel, which likely decreased the amount of in-cylinder regions of high combustion temperature. Reductions in NOx emissions varied from 26% at 2.4 MPa IMEP up to 90% at 0.3 MPa IMEP for ethanol energy fractions of 0.19 and 0.56, respectively.

The lowest levels of ISNOx were attained at 0.3 and 0.6 MPa IMEP due to longer ignition delays and a more homogenous combustion process when compared to the other dual-fuel cases with diesel injections closer to TDC. NOx emissions were decreased when increasing the engine load from 0.9 to 1.5 MPa IMEP because of a later optimum CA50 and thus lower combustion temperatures. At high engine loads of 1.8 and 2.4 MPa IMEP, the ethanol autoignition process and shorter diesel mixing-controlled combustion helped reduce the peak in-cylinder gas temperatures [46], decreasing the ISNOx when compared with those of the CDC operation.

Smoke levels from dual-fuel combustion were maintained comparatively low despite the use of lower diesel injection pressures than the CDC operation (see Section 3). Early diesel injections and high EF curbed fuel rich combustion and limited soot emissions to 0.05 FSN at 0.3 and 0.6 MPa IMEP. However, the levels of soot were increased to 0.235 FSN at 1.5 MPa IMEP. This was likely a result of higher local fuel/air equivalence ratio and reduced combustion temperatures introduced by the shorter ignition delay and later CA50. In the CDC mode, higher diesel injection pressures and in-cylinder gas temperatures helped reduce soot emissions as the engine load was increased.

Net indicated specific emissions of CO (ISCO) and unburnt HC (ISHC) increased significantly in the dual-fuel combustion when compared to the CDC operation. This was possibly a result of premixed fuel trapped in the crevice volumes of the stock diesel piston as well as lower local in-cylinder gas temperatures [6].

High levels of ISCO and ISHC were measured for the dual-fuel operation at 0.3 MPa IMEP. This can be attributed to excessively low combustion temperatures and overly lean regions that did not release

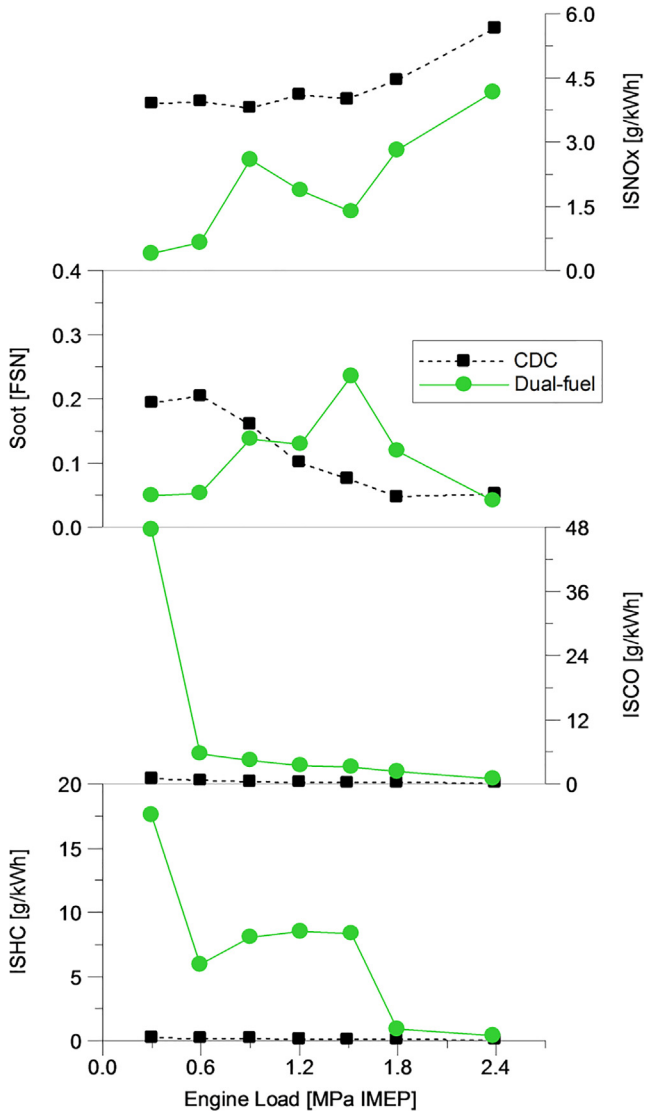

Fig. 8. Engine-out emissions for optimised CDC and ethanol–diesel dual-fuel operation at 1200 rpm.

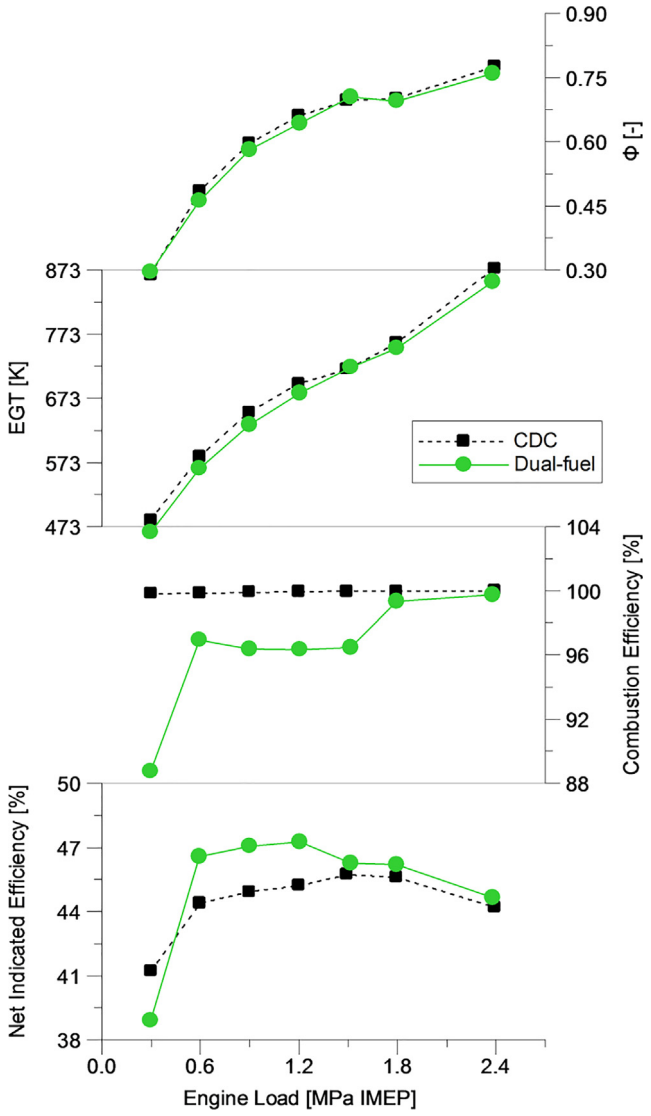

Fig. 9. Engine performance for optimised CDC and ethanol–diesel dual-fuel operation at 1200 rpm.

enough heat in order to effectively oxidise the fuel [6]. At 1.8 and 2.4 MPa IMEP, the use of lower EF as well as lower EGR rates likely increased combustion temperatures, decreasing CO and unburnt HC emissions.

4.5. Engine performance

Fig. 9 depicts the engine performance metrics for optimised CDC and ethanol–diesel dual-fuel operation. The global fuel/air equivalence ratio (Φ) of the dual-fuel combustion was either comparable or lower than that of the CDC mode at a given engine load. This was attributed to minor variations in the intake air flow rate (within 3% and not shown for the sake of brevity) and improvements in net indicated efficiency. Differences in LHV_{fuel} and total fuel flow rate possibly balanced out changes in stoichiometric air/fuel ratio.

Higher exhaust gas temperatures (EGT) were measured as engine load was increased due to later CA90 and higher levels of fuel energy supplied. However, the dual-fuel operation produced EGTs up to 20 K lower than those of the corresponding CDC case. This was perhaps a result of a more homogenous and lower temperature combustion process for an engine operation with premixed ethanol fuel [31,46].

The dual-fuel mode also yielded lower combustion efficiencies than the CDC cases as supported by the higher levels of ISCO and ISHC in Fig. 8. At the lowest load of 0.3 MPa IMEP, a relatively low combustion efficiency of 88.7% adversely affected the performance of the dual-fuel operation, limiting the net indicated efficiency to 38.9% and the EGT to 463 K. This can represent a challenge for HD engine manufacturers due to a reduction in the effectiveness of the oxidation catalyst in reducing CO and unburnt HC emissions [66,67].

In-cylinder control strategies such as intake throttling and iEGR can help increase the EGT while simultaneously minimising the levels of ISCO and ISHC at light engine loads [31]. As the engine load was increased, higher Φ and local in-cylinder gas temperatures helped maintain the combustion efficiency above 96.3% despite the use of ethanol energy fractions of up to 0.79.

Finally, ethanol–diesel dual-fuel combustion resulted in higher net indicated efficiencies than the CDC operation between 0.6 and 2.4 MPa IMEP. A peak net indicated efficiency of 47.2% was attained at 1.2 MPa IMEP and represented an increase of 4.4% over the 45.2% of the CDC mode. The ethanol autoignition process likely helped decrease the combustion temperatures and thus the heat transfer losses [51], as supported by the NOx reduction in Fig. 8.

The use of a late CA50 at 1.5 MPa IMEP and relatively low EF at 1.8 and 2.4 MPa IMEP limited improvements in the net indicated efficiency

of the dual-fuel operation, but were necessary in order to control the PRR below 2.0 MPa/CAD. The maximum net indicated efficiency achieved by the CDC operation was 45.7% at 1.5 MPa IMEP.

4.6. Additional practical considerations

Additional practical aspects for ethanol–diesel dual-fuel operation were assessed in order to evaluate whether the combustion strategy can be successfully used in a Euro VI HD engine. The analysis focused on the total fuel flow rate, estimated consumption of aqueous urea solution in the SCR system ($\dot{m}_{urea}$) to meet the Euro VI NOx limit of 0.4 g/kWh, and SCR corrected net indicated efficiency (*Net Indicated Eff.*$_{SCRcorr.}$). The methodology for the calculation of these performance metrics has been described in our previous study [45], where $\dot{m}_{urea}$ was estimated at 1% of the diesel equivalent fuel flow rate per g/kWh reduction in NOx emissions [24–26]:

$$\dot{m}_{urea} = 0.01(ISNOx-0.4)\left(\dot{m}_{diesel} + \dot{m}_{ethanol}\frac{LHV_{ethanol}}{LHV_{diesel}}\right) \quad (3)$$

Fig. 10 shows the optimised ethanol-diesel dual-fuel combustion increased the total fuel flow rate by up to 45.8% in comparison with the CDC mode (8.12 kg/h vs. 5.57 kg/h at 1.5 MPa IMEP). This is attributed to the relatively lower density ($\rho_{ethanol}$) and energy content ($LHV_{ethanol}$) of the ethanol fuel. The total fuel flow rate dropped when increasing the engine load from 1.5 to 1.8 MPa IMEP due to a reduction in EF. Appropriate volumes of diesel and ethanol fuel tanks will have to be designed according to the application of the engine and duty cycle.

In terms of NOx aftertreatment, the ethanol–diesel dual-fuel combustion attained lower levels of ISNOx than the CDC operation, effectively decreasing the $\dot{m}_{urea}$ required. Higher $\dot{m}_{urea}$ were estimated for both the combustion modes as the engine load was increased. This was due to a combination of a higher total fuel flow rate (e.g. increased production of NOx emissions in g/h) with reductions in the EGR rate at 1.8 and 2.4 MPa IMEP.

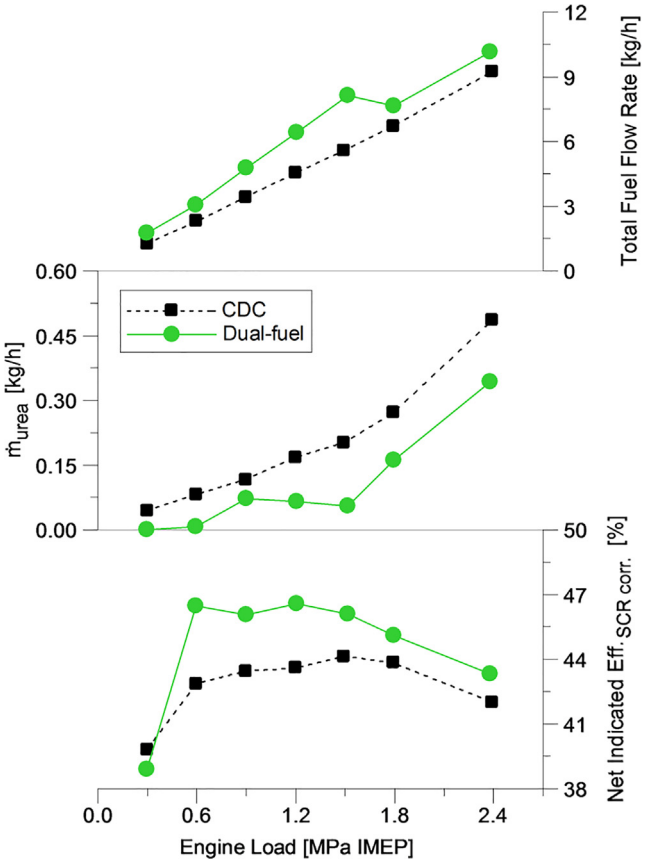

Fig. 10. Practical considerations for optimised CDC and ethanol–diesel dual-fuel operation on a Euro VI HD engine.

The lower urea consumption in the dual-fuel mode allowed for higher *Net Indicated Eff.*$_{SCRcorr.}$ between 0.6 and 2.4 MPa IMEP. The maximum *Net Indicated Eff.*$_{SCRcorr.}$ of 46.5% was achieved at 0.6 MPa IMEP and represented a relative increase of 8.4% over the CDC mode. Lowered combustion efficiency limited the *Net Indicated Eff.*$_{SCRcorr.}$ of the dual-fuel mode at 0.3 MPa IMEP, despite the low engine-out NOx of 0.4 g/kWh and $\dot{m}_{urea} = 0$.

These improvements can reduce the engine running costs depending on the volumetric price ratio between ethanol and diesel fuel [45] as well as the cost of aqueous urea solution. Nevertheless, the implementation of this dual-fuel combustion strategy on a HD engine would have to weigh the higher efficiency and lower NOx emissions against the additional complexity and upfront cost of a port fuel injection system and extra fuel tank.

4.7. Potential CO_2 reduction

The data in Table 4 reveal that the complete combustion of ethanol can reduce the emissions of CO_2 by ~4% when compared against the combustion of diesel at a given energy input. However, practical ethanol energy fractions in dual-fuel mode vary between 0.00 and ~0.80 while the actual fuel energy consumption changes with the net indicated efficiency.

The use of the engine-out CO_2 emissions in the calculation of net indicated specific emissions of CO_2 ($lSCO_2$) would result in incorrect trends for dual-fuel operation, with significant reductions at all engine loads. This is due to the partial oxidation of hydrocarbons, which increase the formation of CO and reduce the concentration of CO_2 in the exhaust stream.

To remove the effect of incomplete combustion, the $lSCO_2$ (in g/kWh) was estimated using Eq. (4), which assumed a complete oxidation of the fuel injected to CO_2, either inside the cylinder or in the aftertreatment system. The CO_2 emissions resulting from aqueous urea solution reactions in the SCR system [26] have been neglected because $\dot{m}_{urea}$ was estimated and its impact on $ISCO_2$ is expected to be very small [68].

$$ISCO_2 = \left(\frac{\dot{m}_{diesel}}{M_{diesel}} + \frac{\dot{m}_{ethanol}}{M_{ethanol}}\right)\left(\frac{M_{CO_2}}{P_{ind}}\right) \times 10^3 \quad (4)$$

where M_{CO_2} is the molar mass of CO_2 of 44.01 g/mol [52] and P_{ind} is the net indicated power in kW.

Fig. 11 shows the optimised dual-fuel operation can achieve lower $lSCO_2$ than the CDC mode from 0.6 to 2.4 MPa IMEP. The potential CO_2 reduction introduced by the ethanol–diesel dual-fuel combustion varied between 1.8% and 7.5%. This improvement was a result of the increase in the net indicated efficiency combined with the higher hydrogen to carbon ratio of the ethanol fuel [69,70]. The low net indicated efficiency at 0.3 MPa IMEP prevented any CO_2 reduction and increased the $lSCO_2$ by 3.7% when compared to the CDC mode.

In order to provide additional insight into the CO_2 reduction, a tank-

Table 4
Hypothetical CO_2 emissions for diesel and ethanol combustion.

Property	Diesel	Ethanol
Normalised molecular composition	$CH_{1.825}O_{0.0014}$	$CH_{3O0.5}$
Lower heating value (LHVfuel)	42.9 MJ/kg	26.9 MJ/kg [51]
Normalised molar mass (Mfuel)	13.87 g/mol	23.03 g/mol
Mass of CO2 emissions per mole of fuel	44.01 gCO_2/mol	44.01 gCO_2/mol
Mass of CO2 emissions per mass of fuel	3.17 gCO_2/g	1.91 gCO_2/g
Mass of CO2 emissions per MJ of fuel	73.9 gCO_2/MJ	71 gCO_2/MJ
Specific CO2 emissions reduction	n/a	~4%

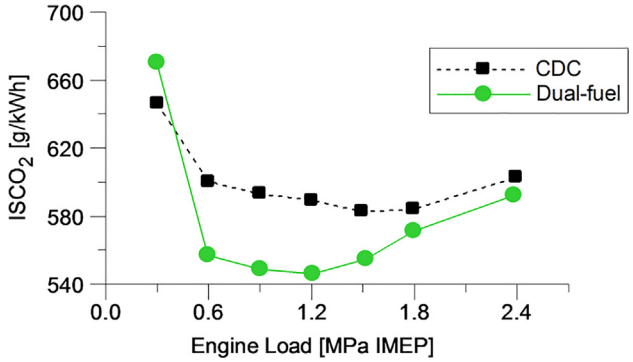

Fig. 11. Estimated $ISCO_2$ for optimised CDC and ethanol–diesel dual-fuel operation at 1200 rpm.

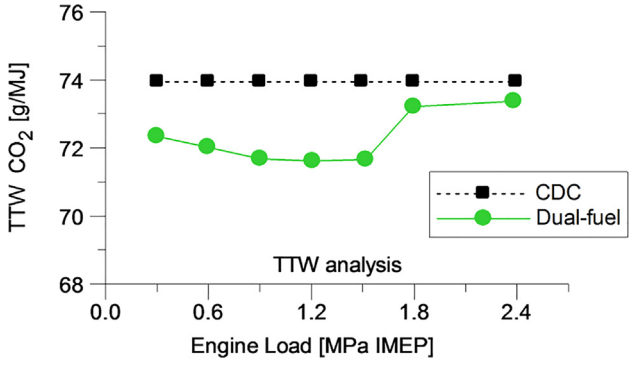

Fig. 12. Estimated TTW CO_2 emissions for CDC and ethanol–diesel dual-fuel operation.

to-wheels (TTW) analysis was performed by calculating the ratio of the estimated mass of CO_2 emissions to the total fuel energy supplied to the engine (in MJ) as

$$TTW\ CO_2 = \frac{ISCO_2 P_{ind}}{(\dot{m}_{diesel} LHV_{diesel} + \dot{m}_{ethanol} LHV_{ethanol})} \quad (5)$$

Fig. 12 indicates the optimised ethanol–diesel dual-fuel combustion reduced the levels of TTW CO_2 emissions by up to 3.2% when compared against a constant 73.9 g/MJ produced by the CDC operation. This was attributed to the usage of the ethanol fuel, as the TTW CO_2 emissions are heavily dependent on the in-cylinder fuel characteristics (e.g. M_{fuel} and LHV_{fuel}).

It is important to note that the data plotted in Figs. 11 and 12 were obtained by assuming complete conversion of the fuel into CO_2. For a more comprehensive analysis, the actual TTW CO_2 emissions should be measured downstream of the aftertreatment system during the appropriate engine/vehicle test cycle.

4.8. Theoretical well-to-wheels analysis

A well-to-wheels (WTW) analysis can be used to assess the GHG emissions and energy expended over the production and use of a given fuel [37,44]. This holistic methodology now combines the TTW results with the well-to-tank (WTT). The WTT takes into consideration the GHGs emitted during the extraction or cultivation of raw materials, processing, transportation, and other processes necessary to physically get the fuel into the fuel tank.

The levels of GHGs were expressed as grams of CO_2 equivalent (CO_{2eq}) emissions per MJ of fuel injected. This was required because of the higher global warming potentials (GWPs) for methane (CH_4) and nitrous oxide (N_2O) compounds, which have GWPs equivalent to 25 and 298 times that of the CO_2 over a time span of 100 years [71].

If one considers that the CO_2 emissions produced from bioethanol combustion can be absorbed by plants during photosynthesis [37,44], the TTW CO_{2eq} emissions for a bioethanol-diesel dual-fuel engine will be determined by those emitted from diesel combustion only:

$$TTW\ CO_{2eq} = 73.9(1-EF) \quad (6)$$

From Eq. (6), the WTW CO_{2eq} emissions were given by

$$WTW\ CO_{2eq} = [WTT_{diesel}(1-EF) + WTT_{ethanol}(EF)] + TTW\ CO_{2eq} \quad (7)$$

where WTT_{diesel} is the WTT CO_{2eq} emissions for fossil diesel fuel of 15.4 g/MJ [38,39] and $WTT_{ethanol}$ is the WTT CO_{2eq} emissions for bioethanol, which varies with the biomass and fuel production process.

Dual-fuel operation WTW CO_{2eq} emissions were calculated for corn ethanol produced in the United States ($WTT_{ethanol}$ of 68.9 g/MJ [38,39]); wheat ethanol produced in the European Union with production energy provided by a natural gas-fired combined heat and power plant ($WTT_{ethanol}$ of 64.8 g/MJ [38,39]); and sugarcane ethanol produced in Brazil ($WTT_{ethanol}$ of 24.8 g/MJ [38,39]).

It must be noted that $WTT_{ethanol}$ excluded CO_{2eq} emissions produced by indirect land use change (iLUC). This is due to the uncertainty over the predictions [72–75] and the potential bonus if biomass is obtained from restored degraded land [36].

Fig. 13 shows the theoretical TTW CO_{2eq} and WTW CO_{2eq} emissions for both engine operating modes. Bioethanol-diesel dual-fuel combustion yielded lower TTW CO_{2eq} emissions than the CDC mode. The lowest TTW CO_{2eq} emissions were attained at mid-loads, where both the net indicated efficiency and EF were maximised.

The relatively lower TTW CO_{2eq} emissions helped decrease the WTW CO_{2eq} emissions resulting from bioethanol-diesel dual-fuel operation. However, the biomass feedstock significantly affected the CO_{2eq} reduction benefit, which highlights the importance of the source of the biofuel.

Dual-fuel combustion with sugarcane ethanol demonstrated the best results, decreasing the WTW CO_{2eq} emissions by up to 57% in comparison with the 89.3 g/MJ for a CDC operation. The reductions in TTW CO_{2eq} and WTW CO_{2eq} emissions can help combat climate change and

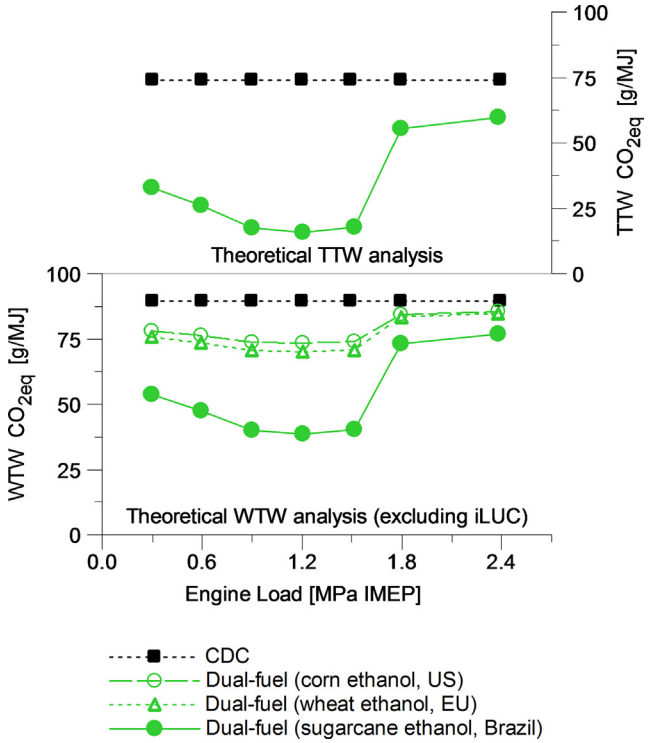

Fig. 13. Theoretical TTW and WTW CO_{2eq} emissions for CDC and bioethanol-diesel dual-fuel operation.

achieve a more sustainable energy source for the transport sector.

5. Conclusions

In this study, experiments were performed to compare the controllability, exhaust emissions, and fuel conversion efficiency of ethanol–diesel dual-fuel combustion to those of conventional diesel combustion (CDC). The investigation was conducted using identical operating conditions at a constant engine speed of 1200 rpm and different loads ranging between 0.3 and 2.4 MPa IMEP.

Testing was carried out on a HD diesel engine with a stock piston and compression ratio of 16.8. Peak in-cylinder pressure and pressure rise rate (PRR) were limited at 18 MPa and 2.0 MPa/CAD, respectively. The diesel injection timings and fuel delivery were optimised for the maximum net indicated efficiency in both the combustion modes. The comparison against the CDC operation allowed for a better understanding of the potentials, requirements, and limitations of the ethanol–diesel dual-fuel combustion, which can be summarised as follows:

1. The dual-fuel combustion attained significantly lower NOx and soot emissions than the CDC cases at low engine loads of 0.3 and 0.6 MPa IMEP. This was attributed to the combustion of a more homogeneous charge obtained by the use of an early single diesel injection at approximately -36 CAD ATDC and large percentages of premixed ethanol (with energy fractions of 0.56 and 0.65).
2. The dual-fuel mode experienced a relatively low net indicated efficiency of 38.9% at the lowest load of 0.3 MPa IMEP. This was associated with the reduced combustion efficiency of 88.7% caused by excessively lean and low temperature combustion. This region of engine speed-load map also suffered from a low exhaust gas temperature of 463 K, which can adversely affect the effectiveness of the oxidation catalyst.
3. Higher ethanol energy fractions of up to 0.79 and different diesel injections were required as the engine load was increased from 0.6 to 1.5 MPa IMEP. A transition zone was observed between 0.6 and 0.9 MPa IMEP where less diesel fuel could be partially premixed in order to avoid early ignition and control the levels of PRR.
4. At mid-loads of 0.9, 1.2, and 1.5 MPa IMEP, optimised dual-fuel combustion was achieved with a 3 mm^3 diesel pre-injection prior to the main diesel injection. The relatively higher degree of fuel stratification increased the levels of NOx and soot when compared to those obtained at low engine loads. Nevertheless, mid-load dual-fuel operation attained lower NOx emissions and up to 4.4% higher net indicated efficiencies than the CDC cases.
5. At high engine loads of 1.8 and 2.4 MPa IMEP, early autoignition of the ethanol fuel increased the PRR and limited the maximum ethanol energy fractions to 0.25 and 0.19, respectively. This was linked to the high in-cylinder gas temperatures and pressures prior to the start of combustion. Nonetheless, the ethanol compression ignition combustion helped increase the net indicated efficiency and reduce NOx emissions in comparison with the CDC mode. This was primarily due to a shorter diesel mixing-controlled combustion.
6. The ethanol–diesel dual-fuel combustion increased the total fuel flow rate by up to 45.8% when compared to the CDC operation. This was a result of the differences in fuel characteristics (e.g. LHV_{fuel}) and will require the design of appropriate fuel tank volumes.

Overall, the optimisation of the diesel injection strategy and ethanol energy fraction was a key enabler for controlling the PRR. This allowed for dual-fuel combustion with higher net indicated efficiencies than the CDC operation between 0.6 and 2.4 MPa IMEP, with a peak of 47.2% at 1.2 MPa IMEP. Furthermore, the ethanol–diesel dual-fuel combustion attained lower NOx emissions (up to 90%) than the CDC mode from low to full engine load. This can decrease the consumption of aqueous urea solution in the exhaust aftertreatment system and help to lower the engine running cost. Finally, the substitution of diesel in favour of bioethanol (e.g. produced from sugarcane) can reduce the use of fossil fuels and effectively minimise the GHG emissions of future HD engines, as supported by the lower tank-to-wheels and well-to-wheels CO_2 equivalent emissions.

Acknowledgments

V.B. Pedrozo would like to acknowledge CAPES Foundation (Coordenação de Aperfeiçoamento de Pessoal de Nível Superior), research grant No. 13455/13–03, for supporting his PhD study at Brunel University London under the supervision of Prof. Hua Zhao. V.B. Pedrozo also would like to thank J.C. Bridi, M. Dalla Nora, M. Dhanji, and W.H. Au for the comments on the manuscript.

References

[1] Intergovernmental Panel on Climate Change (IPCC). Climate Change 2014 – Synthesis Report. IPCC Fifth Assessment Report 2015: 1–112.
[2] United States Environmental Protection Agency. Climate Change Indicators: Atmospheric Concentrations of Greenhouse Gases. EPA's Climate Change Indicators 2016. https://www.epa.gov/climate-indicators/climate-change-indicators-atmospheric-concentrations-greenhouse-gases (accessed 4.07.17).
[3] Miller JD, Façanha C. The state of clean transport policy - A 2014 synthesis of vehicle and fuel policy developments. The ICCT Report 2014: 73.
[4] Kodjak, D. Policies to reduce fuel consumption, air pollution, and carbon emissions from vehicles in G20 nations. The ICCT Briefing Paper 2015: 28.
[5] Dec JE. A conceptual model of DI diesel combustion based on laser sheet imaging. SAE Technical Paper; 1997. doi: 10.4271/970873.
[6] Kokjohn SL, Hanson RM, Splitter Da, Reitz RD. Fuel reactivity controlled compression ignition (RCCI): a pathway to controlled high-efficiency clean combustion. Int J Eng Res 2011;12:209–26. http://dx.doi.org/10.1177/1468087411401548.
[7] Musculus MPB, Miles PC, Pickett LM. Conceptual models for partially premixed low-temperature diesel combustion. Prog Energy Combus Sci 2013;39. http://dx.doi.org/10.1016/j.pecs.2012.09.001.
[8] Reitz RD. Directions in internal combustion engine research. Combust Flame 2013;160:1–8. http://dx.doi.org/10.1016/j.combustflame.2012.11.002.
[9] Iwabuchi Y, Kawai K, Shoji T, Takeda Y. Trial of new concept diesel combustion system - premixed compression-ignited combustion. SAE Tech Paper 1999. http://dx.doi.org/10.4271/1999-01-0185.
[10] World Health Organization. WHO Air quality guidelines for particulate matter, ozone, nitrogen dioxide and sulfur dioxide; 2006.
[11] World Health Organization. Global health risks – Mortality and burden of disease attributable to selected major risks. Genova; 2009.
[12] Environmental Protection Agency (EPA) – National Highway Traffic Safety Administration (NHTSA) - Department of Transportation (DOT). Greenhouse Gas Emissions and Fuel Efficiency Standards for Medium- and Heavy-Duty Engines and Vehicles. Federal Register – Rules and Regulations 2011; 76.
[13] Environmental Protection Agency (EPA) – National Highway Traffic Safety Administration (NHTSA) – Department of Transportation (DOT). Greenhouse Gas Emissions and Fuel Efficiency Standards for Medium- and Heavy-Duty Engines and Vehicles – Phase 2. Federal Register – Rules and Regulations 2016; 81.
[14] The European Parliament and the Council of the European Union. Regulation (EC) No 595/2009. Official Journal of the European Union 2009; 188.
[15] The European Parliament and the Council of the European Union. Commission Regulation (EU) No 582/2011. Official Journal of the European Union 2011; 167.
[16] Posada F, Chambliss S, Blumberg K. Costs of emission reduction technologies for heavy-duty diesel vehicles. The ICCT White Paper 2016.
[17] Delgado O, Rodríguez F, Muncrief R. Fuel Efficiency Technology in European Heavy-Duty Vehicles: Baseline and Potential for the 2020–2030 Time Frame. The ICCT White Paper; 2017.
[18] Görsmann C. Improving air quality while reducing the emission of greenhouse gases. Johnson Matthey Technol Rev 2015;59:139–51. http://dx.doi.org/10.1595/205651315X687524.
[19] O'Connor J, Borz M, Ruth D, Han J, Paul C, Imren A, et al. Optimization of an Advanced Combustion Strategy Towards 55% BTE for the Volvo SuperTruck Program. SAE International Journal of Engines 2017; 10: 2017–01 – 0723. doi: 10.4271/2017-01-0723.
[20] Stanton D, Charlton S, Vajapeyazula P. Diesel Engine Technologies Enabling Powertrain Optimization to Meet U.S. Greenhouse Gas Emissions. SAE International Journal of Engines 2013; 6. doi:10.4271/2013-24-0094.
[21] López – De Jesús YM, Chigada PI, Watling TC, Arulraj K, Thorén A, Greenham N, et al. NOx and PM Reduction from Diesel Exhaust Using Vanadia SCRF®. SAE International Journal of Engines 2016;9:2016–01 – 0914. doi: 10.4271/2016-01-0914.
[22] Walker A, Johnson Matthey. Catalyst-Based Emission Control Solutions for the Global HDD Market – What Does the Future Hold? Presentation at SAE 2016 Heavy-Duty Diesel Emissions Control Symposium, Gothenburg: 2016.
[23] Delgado O, Lutsey N. The U.S. SuperTruck Program: Expediting the development of advanced heavy-duty vehicle efficiency technologies. The ICCT White Paper 2014.
[24] Charlton S, Dollmeyer T, Grana T. Meeting the US Heavy-Duty EPA 2010 Standards and Providing Increased Value for the Customer. SAE International Journal of

Commercial Vehicles 2010; 3. doi: 10.4271/2010-01-1934.
[25] Johnson TV. Diesel Emissions in Review. SAE International Journal of Engines 2011; 4. doi:10.4271/2011-01-0304.
[26] Stanton DW. Systematic development of highly efficient and clean engines to meet future commercial vehicle greenhouse gas regulations. SAE Int J Eng 2013;6. http://dx.doi.org/10.4271/2013-01-2421.
[27] Liu J, Wang H, Zheng Z, Zou Z, Yao M. Effects of different turbocharging systems on performance in a HD diesel engine with different emission control technical routes. SAE Tech Paper 2016. http://dx.doi.org/10.4271/2016-01-2185.
[28] Dallmann T, Menon A. Technology Pathways for Diesel Engines Used in Non-Road Vehicles and Equipment. The ICCT White Paper; 2016.
[29] Pedrozo VB, May I, Dalla Nora M, Cairns A, Zhao H. Experimental analysis of ethanol dual-fuel combustion in a heavy-duty diesel engine: an optimisation at low load. Appl Energy 2016;165:166–82. http://dx.doi.org/10.1016/j.apenergy.2015.12.052.
[30] Pedrozo VB, May I, Zhao H. Characterization of Low Load Ethanol Dual-Fuel Combustion using Single and Split Diesel Injections on a Heavy-Duty Engine. SAE Tech Paper 2016. http://dx.doi.org/10.4271/2016-01-0778.
[31] Pedrozo VB, May I, Lanzanova TDM, Zhao H. Potential of internal EGR and throttled operation for low load extension of ethanol–diesel dual-fuel reactivity controlled compression ignition combustion on a heavy-duty engine. Fuel 2016;179:391–405. http://dx.doi.org/10.1016/j.fuel.2016.03.090.
[32] Tong D, Ren S, Li Y, Wang Z, Zhang H, Wang Z, et al. Performance and emissions of gasoline Homogeneous Charge Induced Ignition (HCII) by diesel through whole operating range on a heavy-duty multi-cylinder engine. Fuel 2017;197:259–71. http://dx.doi.org/10.1016/j.fuel.2017.02.003.
[33] Divekar P, Han X, Tan Q, Asad U, Yanai T, Chen X, et al. Mode switching to improve low load efficiency of an ethanol-diesel dual-fuel engine. SAE Tech Paper 2017. http://dx.doi.org/10.4271/2017-01-0771.
[34] May I, Pedrozo V, Zhao H, Cairns A, Whelan S, Wong H, et al. Characterization and potential of premixed dual-fuel combustion in a heavy duty natural gas/diesel engine. SAE Tech Paper 2016. http://dx.doi.org/10.4271/2016-01-0790.
[35] Li J, Yang W, Zhou D. Review on the management of RCCI engines. Renew Sustain Energy Rev 2017;69:65–79. http://dx.doi.org/10.1016/j.rser.2016.11.159.
[36] The European Parliament and the Council of the European Union. Directive 2009/28/EC. Official Journal of the European Union 2009; 140.
[37] Edwards R, Larivé J-F, Rickeard D, Weindorf W. Well-to-Wheels analysis of future automotive fuels and powertrains in the European context: Well-to-Tank Report – Version 4.a. Joint Research Centre of the European Commission, EUCAR, and CONCAWE 2014; 4.a. doi: 10.2790/95629.
[38] Edwards R, Larivé J-F, Rickeard D, Weindorf W. Well-to-Wheels analysis of future automotive fuels and powertrains in the European context: Well-to-Tank Appendix 2 - Version 4a. Joint Research Centre of the European Commission, EUCAR, and CONCAWE; 2014: 1–133. doi:10.2790/95629.
[39] Edwards R, Hass H, Larivé J-F, Rickeard D, Weindorf W. Well-to-Wheels analysis of future automotive fuels and powertrains in the European context: Well-to-Tank Appendix 4 - Version 4a. Joint Research Centre of the European Commission, EUCAR, and CONCAWE 2014. doi:10.2790/95629.
[40] Jaiswal D, De Souza AP, Larsen S, LeBauer DS, Miguez FE, Sparovek G, et al. Brazilian sugarcane ethanol as an expandable green alternative to crude oil use. Nat Clim Change 2017;7:788–92. http://dx.doi.org/10.1038/nclimate3410.
[41] García a, Pastor JM, Belarte E, Balloul I. Operating range extension of RCCI combustion concept from low to full load in a heavy-duty engine. Appl Energy 2015;143:211–27. http://dx.doi.org/10.1016/j.apenergy.2015.01.035.
[42] Benajes J, García A, Monsalve-Serrano J, Boronat V. Achieving clean and efficient engine operation up to full load by combining optimized RCCI and dual-fuel diesel-gasoline combustion strategies. Energy Convers Manage 2017;136:142–51. http://dx.doi.org/10.1016/j.enconman.2017.01.010.
[43] Benajes J, García A, Monsalve-Serrano J, Boronat V. Gaseous emissions and particle size distribution of dual-mode dual-fuel diesel-gasoline concept from low to full load. Appl Therm Eng 2017;120:138–49. http://dx.doi.org/10.1016/j.applthermaleng.2017.04.005.
[44] Ramachandran S, Stimming U. Well to wheel analysis of low carbon alternatives for road traffic. Energy Environ Sci 2015;8:3313–24. http://dx.doi.org/10.1039/C5EE01512J.
[45] Pedrozo VB, May I, Zhao H. Exploring the mid-load potential of ethanol-diesel dual-fuel combustion with and without EGR. Appl Energy 2017;193:263–75. http://dx.doi.org/10.1016/j.apenergy.2017.02.043.
[46] Pedrozo VB, Zhao H. Improvement in high load ethanol-diesel dual-fuel combustion by Miller cycle and charge air cooling. Appl Energy 2018;210:138–51. http://dx.doi.org/10.1016/j.apenergy.2017.10.092.
[47] Schwoerer J, Kumar K, Ruggiero B, Swanbon B. Lost-Motion VVA Systems for Enabling Next Generation Diesel Engine Efficiency and After-Treatment Optimization. SAE Tech Paper 2010. http://dx.doi.org/10.4271/2010-01-1189.
[48] Melo TCC de, Brito MFM de, Moreira MF, Machado GB, Fleischman R. Calculation of Uncertainty of Measurement for Diesel Engine ESC Test Emissions. SAE Technical Paper; 2013.
[49] Joint Committee For Guides In Metrology (JCGM). Evaluation of measurement data – Guide to the expression of uncertainty in measurement. JCGM 100:2008 (GUM 1995 with Minor Corrections); 2008. https://www.bipm.org/en/publications/guides/gum.html.
[50] International Organisation of Legal Metrology (IOLM). International Recommendation No22 - Alcoholometry. First Ed. Paris: 1973.
[51] Heywood JB. Internal Combustion Engine Fundamentals. First Ed. McGraw-Hill, Inc.; 1988.
[52] Economic Commission for Europe of the United Nations (UN/ECE). Regulation No 49 – Uniform provisions concerning the measures to be taken against the emission of gaseous and particulate pollutants from compression-ignition engines and positive ignition engines for use in vehicles. Official Journal of the European Union 2013; 171.
[53] Kar K, Cheng WK. Speciated Engine-Out Organic Gas Emissions from a PFI-SI Engine Operating on Ethanol/Gasoline Mixtures. SAE International Journal of Fuels and Lubricants 2009; 2. doi: 10.4271/2009-01-2673.
[54] Wallner T. Correlation Between Speciated Hydrocarbon Emissions and Flame Ionization Detector Response for Gasoline/Alcohol Blends. J Eng Gas Turb Power 2011;133. http://dx.doi.org/10.1115/1.4002893.
[55] Prikhodko VY, Curran SJ, Barone TL, Lewis Sa, Storey JM, Cho K, et al. Emission characteristics of a diesel engine operating with in-cylinder gasoline and diesel fuel blending. SAE Tech Paper 2010;3:946–55.
[56] Dempsey A, Curran S, Storey J, Eibl M, Pihl J, Prikhodko V, et al. Particulate matter characterization of reactivity controlled compression ignition (RCCI) on a light duty engine. SAE Tech Paper 2014. http://dx.doi.org/10.4271/2014-01-1596.
[57] Benajes J, Garcia A, Monsalve-Serrano J, Boronat V. Particulates size distribution of reactivity controlled compression ignition (RCCI) on a medium-duty engine fueled with diesel and gasoline at different engine speeds. SAE Int J Eng 2017;10. http://dx.doi.org/10.4271/2017-24-0085. 2017–24–0085.
[58] Benajes J, García A, Monsalve-Serrano J, Boronat V. An investigation on the particulate number and size distributions over the whole engine map from an optimized combustion strategy combining RCCI and dual-fuel diesel-gasoline. Energy Convers Manage 2017;140:98–108. http://dx.doi.org/10.1016/j.enconman.2017.02.073.
[59] Storey JM, Curran SJ, Lewis Sa, Barone TL, Dempsey aB, Moses-DeBusk M, et al. Evolution and current understanding of physicochemical characterization of particulate matter from reactivity controlled compression ignition combustion on a multicylinder light-duty engine. Int J Eng Res 2016. http://dx.doi.org/10.1177/146808741666163.
[60] May IA. An experimental investigation of lean-burn dual-fuel combustion in a heavy duty diesel engine. Brunel University London; 2017.
[61] He X, Durrett RP, Sun Z. Late intake valve closing as an emissions control strategy at tier 2 Bin 5 engine-out NOx level. SAE Int J Eng 2008;1. http://dx.doi.org/10.4271/2008-01-0637. 2008–01 – 0637.
[62] Ickes A, Hanson R, Wallner T. Impact of effective compression ratio on gasoline-diesel dual-fuel combustion in a heavy-duty engine using variable valve actuation. SAE Tech Paper 2015. http://dx.doi.org/10.4271/2015-01-1796.
[63] Zhao H. Advanced direct injection combustion engine technologies and development – Volume 2: Diesel engines. Cambridge: Woodhead Publishing Limited; 2010.
[64] Park C, Busch S. The influence of pilot injection on high-temperature ignition processes and early flame structure in a high-speed direct injection diesel engine. Int J Engine Res 2017. http://dx.doi.org/10.1177/1468087417728630.
[65] Desantes JM, Benajes J, García A, Monsalve-Serrano J. The role of the in-cylinder gas temperature and oxygen concentration over low load reactivity controlled compression ignition combustion efficiency. Energy 2014;78:854–68. http://dx.doi.org/10.1016/j.energy.2014.10.080.
[66] Tsang KS, Zhang ZH, Cheung CS, Chan TL. Reducing emissions of a diesel engine using fumigation ethanol and a diesel oxidation catalyst. Energy Fuels 2010;24. http://dx.doi.org/10.1021/ef100899z.
[67] Prikhodko VY, Curran SJ, Parks JE, Wagner RM. Effectiveness of diesel oxidation catalyst in reducing HC and CO emissions from reactivity controlled compression ignition. SAE Int J Fuel Lubr 2013;6. http://dx.doi.org/10.4271/2013-01-0515.
[68] Stelwagen U, Ligterink N. CO2 emission from urea consumption in SCR after-treatment systems in heavy-duty vehicles. TNO Report (TNO 2014 R11513) 2014. http://www.emissieregistratie.nl/erpubliek/documenten/Lucht (Air)/Verkeer en Vervoer (Transport)/Wegverkeer/TNO (2014) CO2 emission from urea consumption in SCR after-treatment systems in HD vehicles.pdf (accessed 2.05.18.).
[69] Di Blasio G, BeatriceS. C, Molina M. Effect of port injected ethanol on combustion characteristics in a dual-fuel light duty diesel engine. SAE Tech Paper 2013;01. http://dx.doi.org/10.4271/2013-01-1692.
[70] Han X, Yang Z, Wang M, Tjong J, Zheng M. Clean combustion of n-butanol as a next generation biofuel for diesel engines. Appl Energy 2016. http://dx.doi.org/10.1016/j.apenergy.2016.12.059.
[71] Intergovernmental Panel on Climate Change (IPCC). Climate Change 2007: The Physical Science Basis. Contribution of Working Group I to the Fourth Assessment Report of the Intergovernmental Panel on Climate Change; 2007.
[72] Laborde D. Assessing the Land Use Change Consequences of European Biofuel Policies. International Food Policy Institute (IFPRI); 2011.
[73] Wang M, Han J, Dunn JB, Cai H, Elgowainy A. Well-to-wheels energy use and greenhouse gas emissions of ethanol from corn, sugarcane and cellulosic biomass for US use. Environ Res Lett 2012;7:045905. http://dx.doi.org/10.1088/1748-9326/7/4/045905.
[74] Yan X, Boies AM. Quantifying the uncertainties in life cycle greenhouse gas emissions for UK wheat ethanol. Environ Res Lett 2013;8:015024. http://dx.doi.org/10.1088/1748-9326/8/1/015024.
[75] Morganti K, Al-Abdullah M, Alzubail A, Kalghatgi G, Viollet Y, Head R, et al. Synergistic engine-fuel technologies for light-duty vehicles: fuel economy and Greenhouse Gas Emissions. Appl Energy 2017;208:1538–61. http://dx.doi.org/10.1016/j.apenergy.2017.08.213.